Journal of Atmospheric and Solar-Terrestrial Physics 73 (2011) 1129–1137

Contents lists available at ScienceDirect

Journal of Atmospheric and Solar-Terrestrial Physics

journal homepage: www.elsevier.com/locate/jastp

Rolling motion in erupting prominences observed by STEREO

Olga Panasenco [a,*], Sara Martin [a], Anand D. Joshi [b], Nandita Srivastava [b]

[a] Helio Research, La Crescenta, CA, USA
[b] Udaipur Solar Observatory, Physical Research Laboratory, Udaipur, India

ARTICLE INFO

Article history:
Received 2 April 2010
Received in revised form
19 August 2010
Accepted 3 September 2010
Available online 19 September 2010

Keywords:
Sun: chromosphere
Sun: corona
Sun: filaments
Sun: magnetic fields
Sun: photosphere
Sun: prominences

ABSTRACT

We analyze the large-scale dynamical forms of three erupting prominences (filaments) observed by at least one of the two STEREO spacecraft and which reveal evidence of sideways rolling motion beginning at the crest of the erupting filament. We find that all three events were also highly non-radial and occurred adjacent to large coronal holes. For each event, the rolling motion and the average non-radial outward motion of the erupting filament and associated CME were away from a neighboring coronal hole. The location of each coronal hole was adjacent to the outer boundary of the arcade of loops overlying the filaments. The erupting filaments were all more non-radial than the CMEs but in the same general direction. From these associations, we make the hypothesis that the degree of the roll effect depends on the level of force imbalances inside the filament arcade related to the coronal hole and the relative amount of magnetic flux on each side of the filament, while the non-radial motion of the CME is related to global magnetic configuration force imbalances. Our analyses of the prominence eruption best observed from both STEREO-A and STEREO-B shows that its spine retained the thin ribbon-like topology that it had prior to the eruption. This topology allows bending, rolling, and twisting during the early phase of the eruption.

1. Introduction

During prominence eruptions with the roll effect (Martin, 2003), the top of the prominence spine is observed to gradually bend to one side of the spine. This sideways rolling creates twist of opposite sign in the two prominence legs as the prominence continues to ascend. The twist is observed to propagate down each leg (Martin, 2003). The roll effect does not occur in all erupting prominences. However, whenever observed, the roll effect gives us essential information and insight into the three-dimensional structure of some classic observed forms of erupting prominences (Panasenco and Martin, 2008).

Before eruption, essentially all prominence spines have the shape of a narrow, thin ribbon with horizontal threads that bend to become nearly vertical at the ends of the spine. In many Hα observations of quiescent prominences, especially when observed against the solar disk, the spine is not visible, but this description remains valid for prominences observed in 304 Å images (Wang et al., 1998).

To learn more about the roll effect we studied three examples of this dynamic effect in large quiescent prominences observed to erupt above the solar limb in images from the EUVI telescope at 304 Å on the STEREO spacecraft. In one case the prominence eruption was observed by both STEREO A and B. In another example, the prominence eruption was observed only by one of the spacecraft STEREO-B. A third event was observed by STEREO-B and only observed in a few frames from STEREO-A. These three events occurred during solar minimum, i.e. at a time when the Sun displayed very low activity. A description of the eruptions, their associated CMEs and circumstances of their magnetic field environment are presented here.

2. Examples of the roll effect in erupting prominences observed by STEREO

2.1. 2008 December 12

The trajectories in Fig. 1 are of the outer boundaries of the erupting prominence of December 12, 2008 (shown as green lines) and its associated CME (shown by red lines) as seen, respectively, by STEREO-A/EUV 304 Å and STEREO-A/COR1 instruments in the SECCHI suite on board the twin STEREO spacecraft (Howard et al., 2008). These concurrent parts of the eruptive event were conspicuously non-radial as seen at the north-east limb from STEREO-A (Figs. 1 and 2).

In Fig. 1, we superposed outlines of the outer boundaries of the CME and the bright core of the prominence plasma for the different moments during the eruption (as observed by STEREO-A EUVI 304 Å and STEREO-A/COR1, respectively). The non-radial

* Corresponding author.
E-mail address: olgapanasenco@aol.com (O. Panasenco).

1364-6826/$ - see front matter © 2010 Elsevier Ltd. All rights reserved.
doi:10.1016/j.jastp.2010.09.010

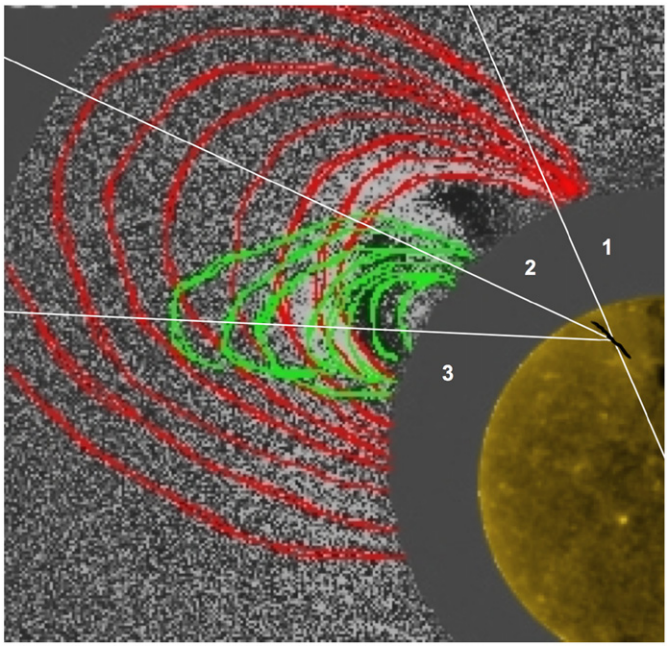

Fig. 1. Non-radial eruption on 2008 December 12. Superposition of the outer boundaries of the CME (red lines) and the erupting prominence inside (green lines) as observed by STEREO-A/COR1 during different moments of the eruption: 07:05, 07:25, 07:45, 08:05, 08:25, 08:45, 09:05 and 09:25 UT. The contour of the filament before eruption is shown by the black line on an image from STEREO-A/EUVI 284 Å. Lines 1, represents the radial line from the prominence site; lines 2 and 3 show the apparent directions of propagation of the CME and erupting prominence, respectively.

propagation is different for the prominence and corresponding CME. The deviation of the CME from the radial propagation is about 40° (the angle between lines 1 and 2) and the difference between the prominence and CME central direction of the eruption is about 20° (the angle between lines 2 and 3).

The erupting prominence is shown in Fig. 2 for a series of times as seen in STEREO-A EIT 304 Å on the NE limb. The orientation of the filament prior to its eruption was nearly parallel with lines of constant latitude. Hence the STEREO-A view is nearly from the west end of the pre-eruptive filament seen against the solar disk. This is an excellent perspective for viewing the rolling motion of the top of the prominence. Prior to its eruption the top of the prominence was nearly vertical above its base. As the top ascended, it also bent southward until the motion of the top is momentarily nearly parallel with the solar surface at 05:46 UT. The rolling motion continued for more than 180°. We are unable to see whether the rolling motion continues after 07:56 UT.

The prominence eruption is not as obviously non-radial as seen at the north-west limb from STEREO-B spacecraft (Fig. 3) because the STEREO-B perspective of the prominence is broadside rather than from one end as for STEREO-A: the separation angle between A and B was 86.7°, which allow to observe the eruption from the two, approximately perpendicular, points of view. Nevertheless, the direction of roll can be recognized and established definitively from the combination of EUVI 304 Å images from the two spacecraft. In the set of images in Fig. 3 from STEREO-B, the roll is toward us as the observers.

It is very clear that the southward rolling motion is accompanied by southward non-radial motion of the overlying corona loop system. As the overlying coronal loops do not participate in the sideways rolling motion of the prominence, we note that the prominence shows a higher degree of non-radial motion than the CME and we suggest this difference is due to its rolling motion. In previous papers on the roll effect (Martin, 2003; Panasenco and Martin, 2008), the associated CMEs were not studied. Therefore, it was not recognized whether the direction of the rolling mass motions could be related to the non-radial motion of the surrounding CME and therefore possibly also related to forces that could cause the whole CME to be non-radial.

The prominence spine prior to eruption was also connected to the disk at each end and also along its sides by threads extending from the filament spine to either side called barbs (Martin, 1998). When a prominence erupts the barbs become detached from the chromosphere. To keep our model of the rolling motion of the prominence simple, we suggest that the barbs threads on opposite sides of the prominence reconnect with each other and collapse back into the spine which retains its ribbon-like topology.

Previously, we have modeled the spine of erupting prominences as flat ribbons that can be bent and twisted (Panasenco and Martin, 2008). We found that the shapes of prominences both before and during eruption could be more closely reproduced by the bending and twisting of a flat ribbon than modeling the prominence mass like a flux tube (Panasenco and Martin, 2008). For this reason, we also empirically model the spine of this erupting filament on December 12, 2008 as a narrow ribbon lying on one edge. The spine is modeled as parallel magnetic threads within the ribbon except where they bend to the chromosphere at their ends. Except at its extreme ends, the ribbon is horizontal and parallel with polarity boundary when it begins to rise slowly prior to its eruption. To create the empirical model of the rolling motion of the prominence spine during the eruption, we first identify the approximate locations of footpoints of the filament at chromosphere in the 304 Å images. Then using the commercial program 3 ds *MAX*, we create a ribbon with the height and length of the filament prior to eruption as seen in 304 Å, (Fig. 4). Next, the model ribbon is distorted in the simplest possible way to match the appearance of the erupting prominence at a given time as seen from the perspective of STEREO-A (Fig. 5a). Then the model Sun with its model prominence is rotated in increments of 18° to show the prominence from different perspectives (Fig. 5b–f). Panel f is the perspective of the empirical prominence model as seen from STEREO-B. We see that our empirical model represents well the outer edge and most of the prominence as seen at STEREO-B. We thus see that our model is useful as a first approximation of the overall topology of the erupting filament.

Since we are able to see the prominence and the CME from both STEREO spacecraft, we can create a three-dimensional representation of both to determine basic spatial information and speeds of parts of the prominence as it erupts. For this purpose, we have used the IDL routine `scc_measure` which employs the tie-pointing technique. Individual features were selected in the prominence mass and in the leading edge of the CME and were traced in most of the images in EUVI 304 Å as well as in the coronagraphs COR1 and COR2 images. A feature in the leading edge was also traced in COR1 and COR2 images. Fig. 6 shows the features in the prominence and in the CME leading edge as seen from COR1 A and B images that were used to carry out the reconstruction. The results from this calculation are shown in the graphs in Fig. 7.

The left panel of Fig. 7 shows the true coordinates of the top of the erupting prominence as seen in EUVI 304 Å observations. The prominence underwent a very gradual rise for more than an hour before its eventual eruption that started at 03:56 UT. This early eruptive phase was also found to be quite slow, its true speed being approximately 50 km/s in the interval from 04:00 to 07:00 UT. A notable change is the decrease in latitude (bottom panel) of the prominence from 47° to 24° once it starts to erupt. Later the prominence, however, was seen to erupt much more rapidly in the coronagraphs COR1 and COR2 images (middle panels), its true speed being around 190 km/s. Whereas a point

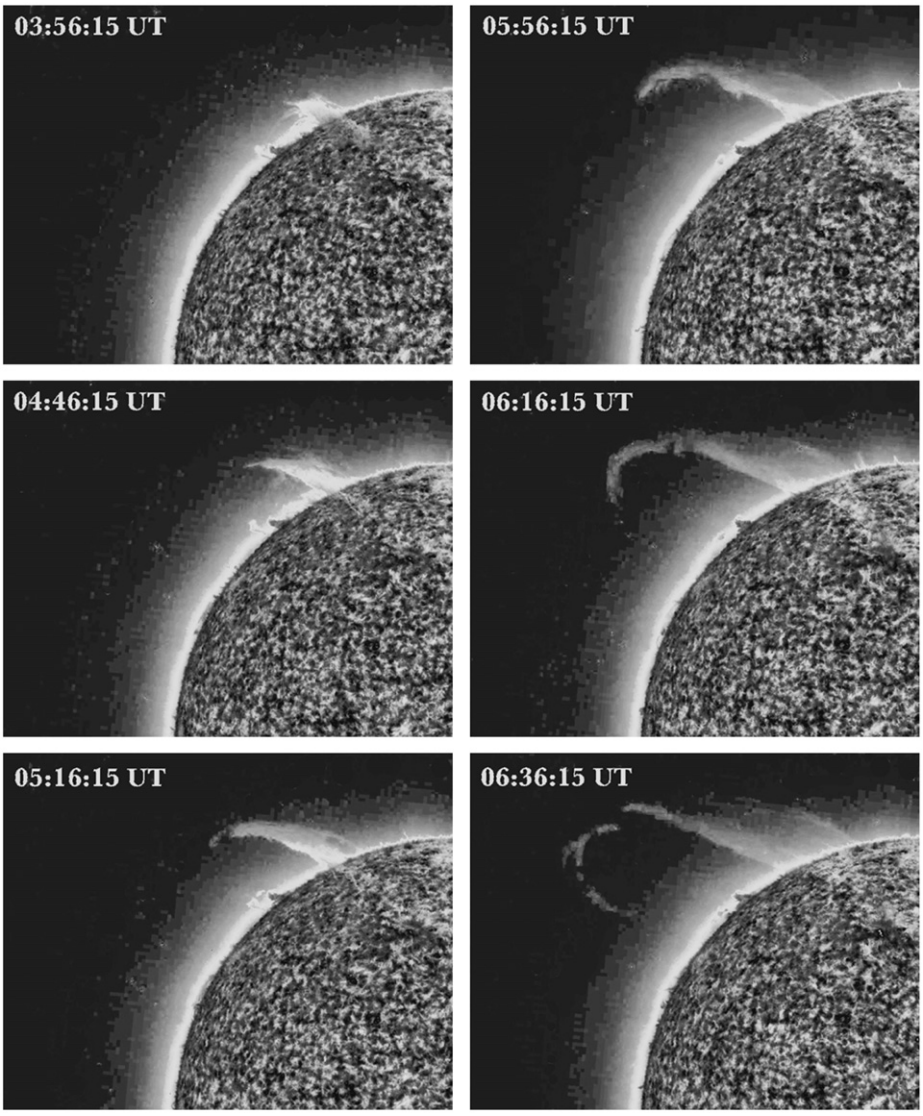

Fig. 2. STEREO-A series showing the roll in the 2008 December 12 event.

selected along the CME leading edge was found to have a still higher true speed of 350 km/s (right panels). However, consistent with the EUVI observations, the decrease in measured latitude concurrent with increasing height was observed in the coronagraphs for both the prominence and the CME (bottom panels). The change in latitude of the leading edge is because of the non-radial motion of the CME. The change in latitude of the prominence is a manifestation of the early phase of roll effect wherein the top of the prominence gradually bends into a shape like the crest of an ocean wave.

2.2. 2009 July 11 and 12

Two erupting prominences with a clear sideways rolling motion in each case were observed on 2009 July 11 and 12, respectively, in the same NE solar quadrant. One eruption occurred at 21:21 UT on July 11 and other at 18:06 UT on July 12 as observed in EUVI images in SECCHI/STEREO.

Fig. 8 (right panel) shows the superposition of the erupting prominence on July 11, 2009 as seen from STEREO-A/EUVI 304 Å and the adjacent polar coronal hole seen by EUVI 171 Å. Fig. 8 (left panel) shows the filament observed in 304 Å on December 12, 2008 superposed on EUVI 171 Å image. Both have a similar spatial relationship to the northern polar coronal hole. In Fig. 8 (left), the polar hole has a conspicuous extension to lower latitudes. In both events, we see that the prominence erupts non-radially away from the adjacent coronal holes.

Fig. 9 compares the eruptions on July 11 and 12 and reveals their opposite directions of the rolling motion as indicated by the curvature of the prominence tops. In the case of the prominence eruption on 2009 July 11, the observed rolling motion was away from the northern polar coronal hole as shown in Fig. 8. For the prominence eruption on 2009 July 12, the rolling motion was away from a coronal hole near the equator. Since the July 12th eruption was observed at the east limb by STEREO-B, the proximity of the erupted prominence to the coronal hole became most clearly visible only 5 days later on July 17, 2009 and this is illustrated in Fig. 10 which is a superposition of the prominences image on July 12 at 304 Å and the STEREO-B 171 Å on July 17, 2009. The projected location of the prominence site relative to the coronal hole is shown by the arrow pointing to a black north-south line representing the latitudes of the prominence as previously seen at the limb on July 12, 2009.

The erupting prominence on July 11, 2009 is primarily seen in EUVI 304 Å images from STEREO-B spacecraft. However, for 5–6 frames between 23:00 and 24:00 UT on July 11, the twisted top of the erupting prominence can be seen in EUVI 304 Å images from

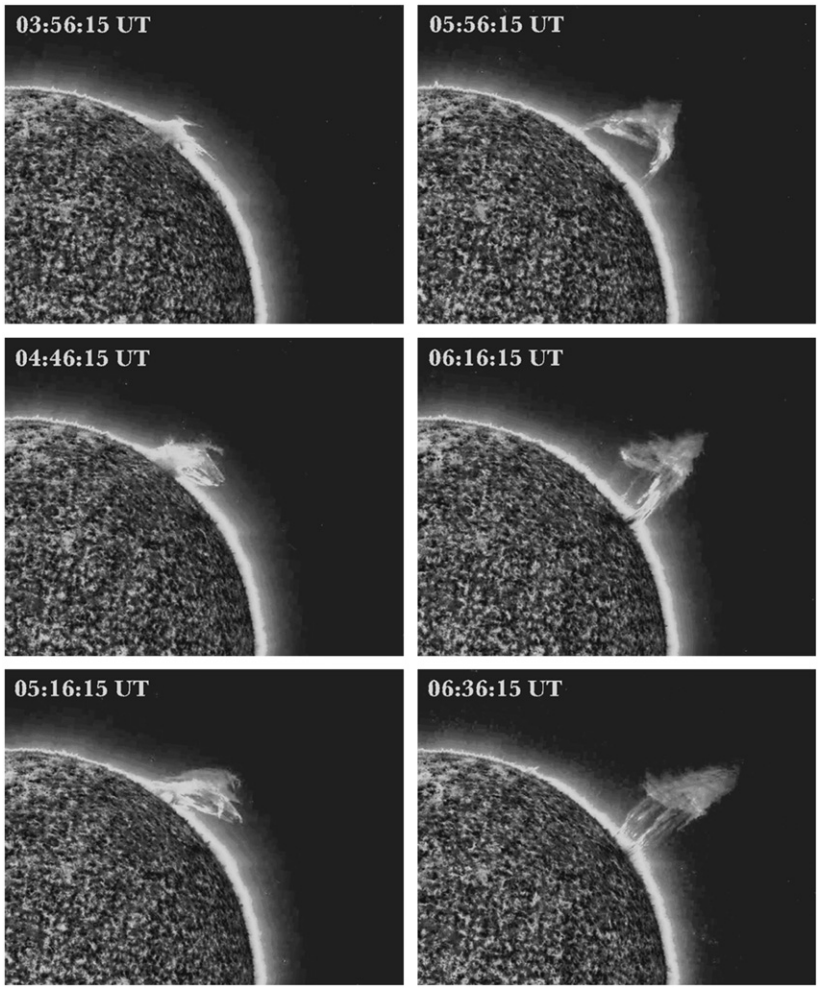

Fig. 3. From the perspective of STEREO-B the roll seen by STEREO-A in Fig. 2 for the same event as on 2008 December 12. The roll is toward the observer and in the direction from the negative to the positive network field side of the filament.

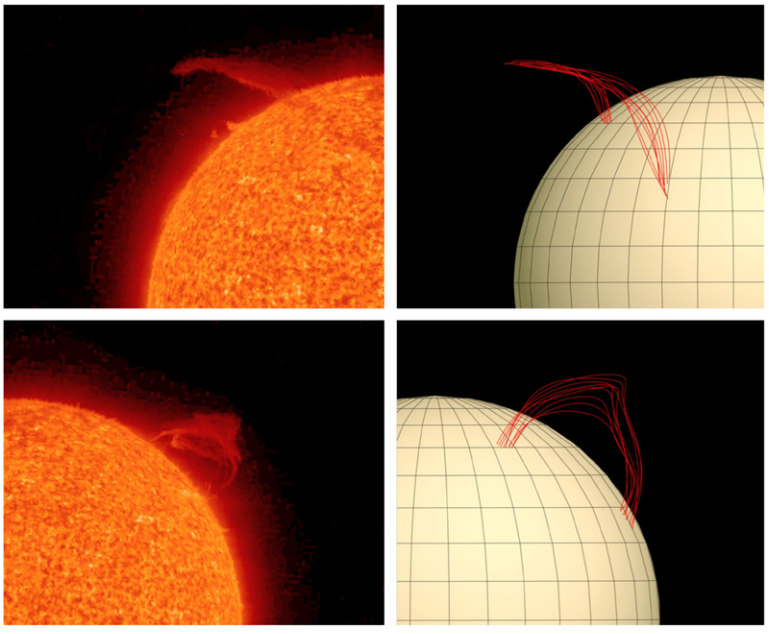

Fig. 4. Roll effect during the eruption on 2008 December 12 (05:36 UT). Top panels: STEREO-A/EUVI 304 Å image and its 3D reconstruction; bottom panels: STEREO- B/EUVI 304 Å image and its 3D reconstruction. The initial bending of the filament ribbon leads to the rolling motion, which is more clearly seen from the perspective of STEREO-A than STEREO-B.

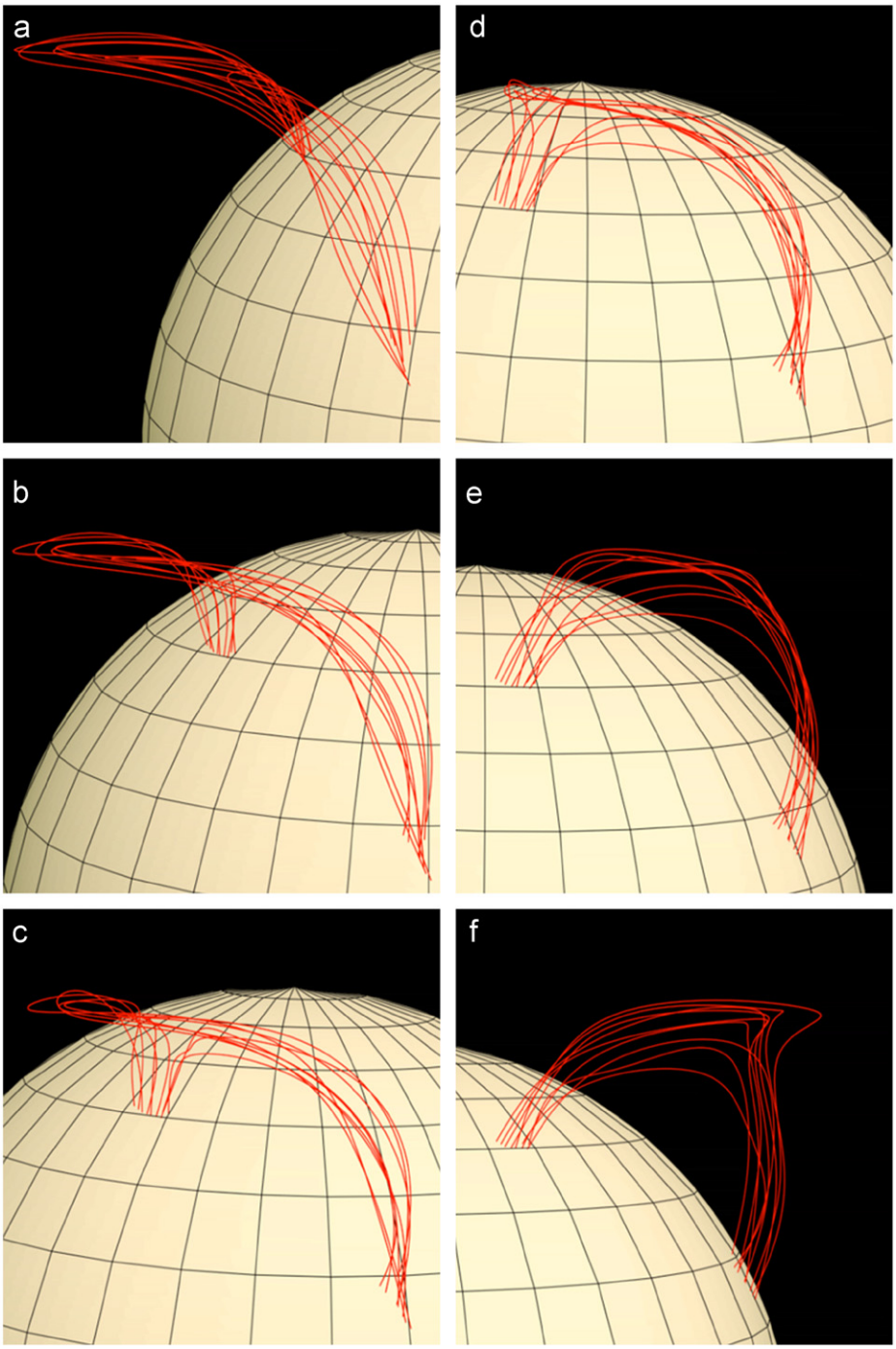

Fig. 5. 3D empirical model of the topology of the prominence eruption on 2008 December 12 (see Fig. 4). The prominence magnetic field topology is represented as a ribbon. The model reveals the apparent changes in shape of the prominence ribbon as seen from different imaginary perspectives. Frames from *a* to *f* show the model as if the Sun were rotated in 18° steps from the observed perspective of STEREO-A in (a) to the perspective from STEREO-B in (f).

STEREO-A as well. The true height of the prominence during this time (between 23:00 and 24:00 UT) was found to be about $1.4R_{\odot}$, while its longitude and latitude were found to be about -165° and 31°, respectively.

3. Potential field calculations of the coronal holes near the erupting prominences

To further investigate whether the relationships of the non-radial motions and rolling motions to the adjacent coronal holes is significant, we looked for a means of depicting the magnetic fields of the coronal holes. Using the potential-field source-surface (PFSS) model with $R_{ss} = 2.5R_{\odot}$ we were able to display the inner-heliospheric magnetic field (Schrijver and De Rosa, 2003) from SOHO/MDI full-disk photospheric magnetograms. Fig. 11 shows the PFSS modeling of the open and closed solar magnetic field for the non-radial eruption on December 12, 2008. In Fig. 11, we compare the curvature of the erupting filaments with the curvature of sets of imaginary field lines. It is seen that the shapes are remarkably similar as if the field of the coronal holes could be guiding the prominence

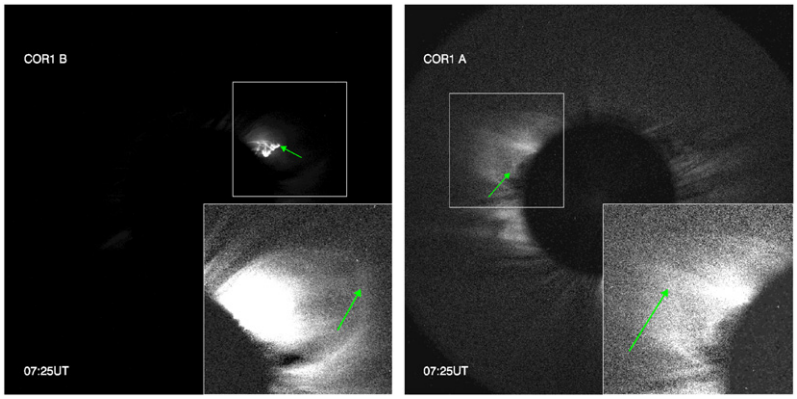

Fig. 6. Features in the prominence and in the CME leading edge on 12 December 2008 event as seen from COR1 B (left image) and COR1 A (right image). These features were used for 3D reconstruction in order to obtain true spatial and speed information of the event. On the COR1 images a feature in the prominence is marked with an arrow, while on the inset images a feature in the CME leading edge is marked with an arrow. The white box shows the location of the inset image on the COR1 A and B images.

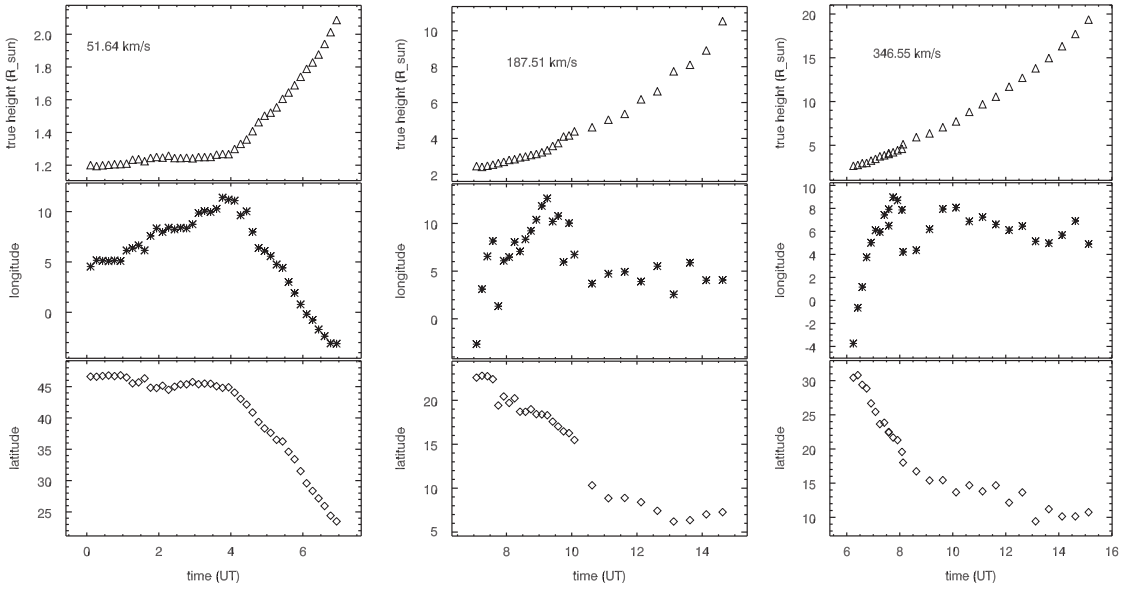

Fig. 7. Left panels: True coordinates of the erupting prominence obtained from EUVI 304 Å observations on 2008 December 12. The speed in top panels are calculated from a 1-D fit to the eruptive phase of the prominence. Middle panels: True coordinates of prominence obtained from combined COR1 and COR2 observations. The same feature in the prominence is followed in images from the two coronagraphs. Right panels: True coordinates of a point in the leading edge of the CME from combined COR1 and COR2 observations. We have tried to follow the same feature in the leading edge in images from the two coronagraphs.

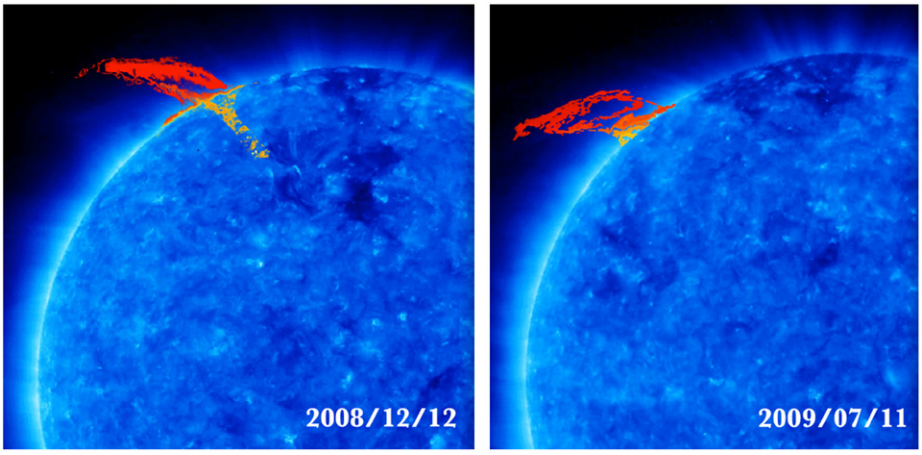

Fig. 8. Superposition of the erupting prominences (STEREO-A/EUVI 304 Å) showing that the prominences are located near the boundary of the north polar coronal hole (STEREO-A/EUVI 171 Å). Non-radial eruption of the prominences on 2008 December 12, 05:36 UT (left) and 2009 July 11, 22:44 UT (right).

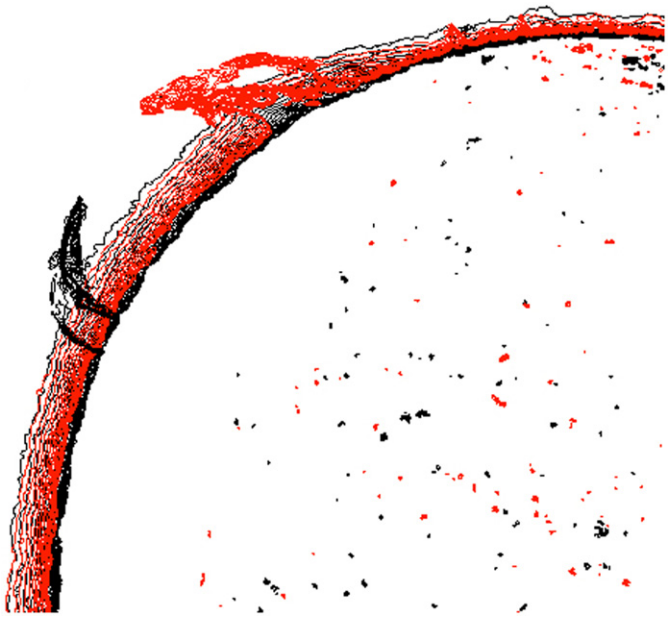

Fig. 9. Non-radial eruptions on July 11, 2009 22:36:15 UT (red) and July 12, 2009 21:01:15 UT (black) from STEREO-B 304 Å. The strong non-radial direction of the poleward prominence eruption is away from the north polar coronal hole and non-radial direction of the more equatorward eruption (in black) is away from an equatorial coronal hole. Two images on these successive days are superposed to compare their non-radial and curvature due to opposite rolling motions of these two eruptions separated in time by approximately one day. (For interpretation of the references to color in this figure legend, the reader is referred to the web version of this article.)

mass parallel with the lower boundary of the coronal holes in each case.

A similar result was noticed by Gopalswamy et al. (2003), Cremades and Bothmer (2004) and Gopalswamy et al. (2009). The central position angle of the structured CMEs was systematically deviated with respect to that of the source regions by about 20° to lower latitudes during the years after solar minimum (1996–1998) (Cremades and Bothmer, 2004). The deflection of structured CMEs is most likely due to the fast solar wind flow from polar coronal holes that encompasses the expansion of CMEs at higher latitudes. At times of higher solar activity the deviations vary in correspondence to the complexity of the corona (Cremades and Bothmer, 2004). It was also found that the CMEs generally move away from the open magnetic field regions. The CME-coronal hole interaction must be widespread in the solar minimum and declining phase (Gopalswamy et al., 2009).

In Fig. 12 we also examine the apparent position of the filament prior to their eruptions on 2009 July 11 and 12 beneath the asymmetric coronal fields generated by the PFSS model. In both cases, the filaments are not centered symmetrically beneath the arcade of overlying coronal loops. Therefore, we suggest—as the filament rises, the magnetic pressure of the filament cavity and overlying arcade is greater on the side of the coronal hole due to limited space for closed field of the arcade at this side (Fig. 13). The initiation of the rolling motion at the top of the prominence is consistent with the prominence responding to a force exerted on the prominence from above. The force is directed more sideward if the filament channel and the filament are not centered beneath the overlying arcade of coronal loops. Decentering of the prominence relative to the arcade is thought to be caused by the imbalance of the distribution of magnetic forces on the two sides of the filament channel (Fig. 13). It seems that the immediate force on the prominence can be only from the cavity and arcade magnetic field.

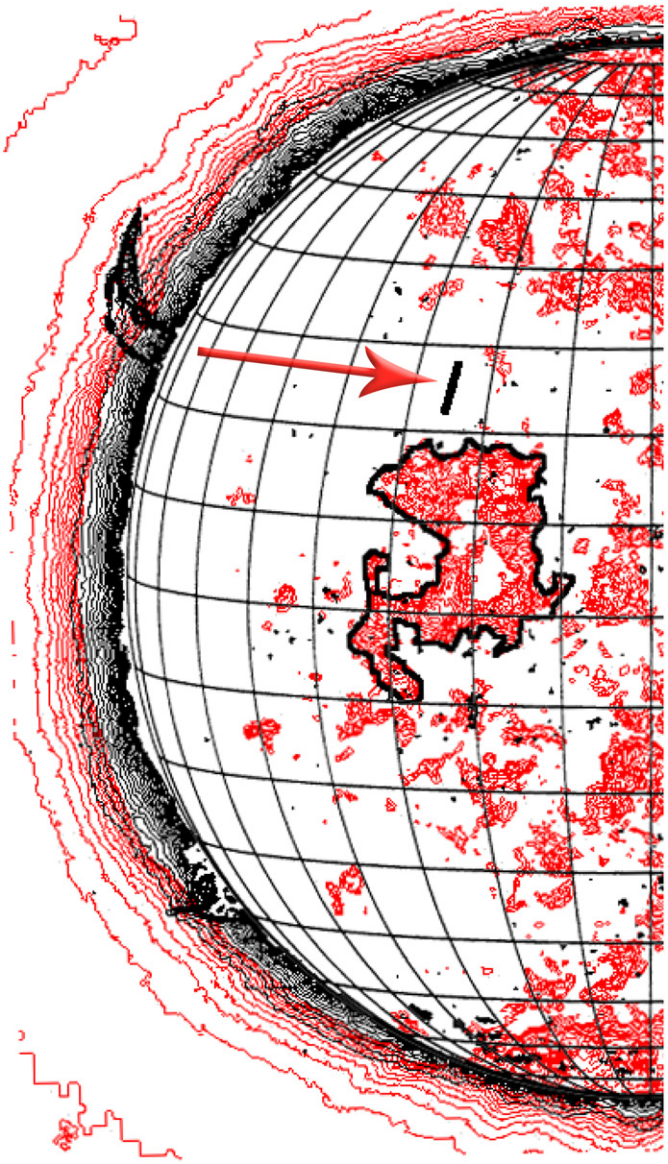

Fig. 10. Non-radial eruption on July 12, 2009 (STEREO-B 304 Å (black)). The strong non-radial direction of the prominence eruption is away from the near-equatorial coronal hole (STEREO-B 171 Å on July 17, 2009) (red). The southern end of the prominence was located within 5° of the northern boundary of this coronal hole (the red hole with the black contour). (For interpretation of the references to color in this figure legend, the reader is referred to the web version of this article.)

There in turn are being affected by deformation of the magnetic field of the CME envelope field which in turn is being distorted by forces associated with the solar wind and coronal hole magnetic fields which represent the global open magnetic field configuration above streamers and pseudostreamers.

4. Discussion

4.1. Physical implication of this study

Our observations confirm the results obtained by Gopalswamy et al. (2003), Cremades and Bothmer (2004) and Gopalswamy et al. (2009) that the deflection of CMEs from the radial direction strongly depends on the topology of either the local and polar coronal holes open field lines which outline the boundaries of the global and local closed magnetic field.

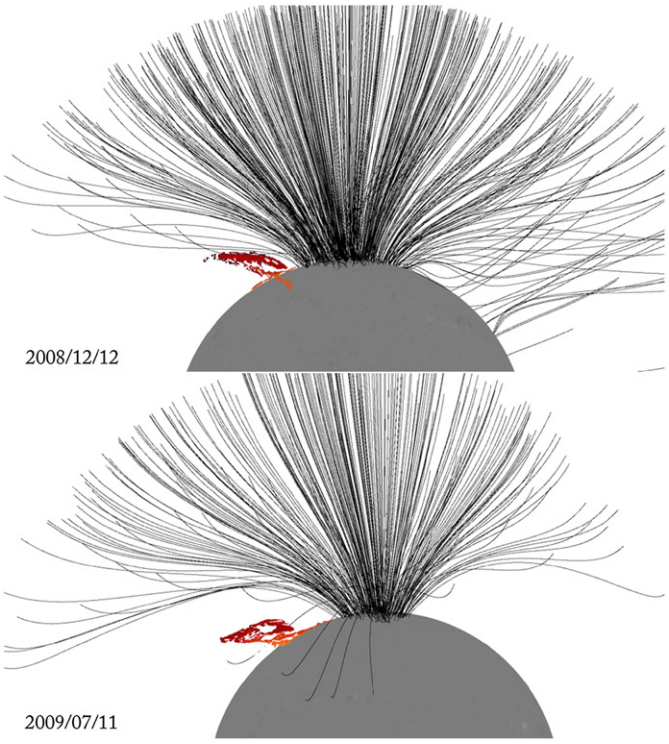

Fig. 11. PFSS extrapolation of the open solar magnetic field for the non-radial eruptions on 2008 December 12 (top) and 2009 July 11 (bottom).

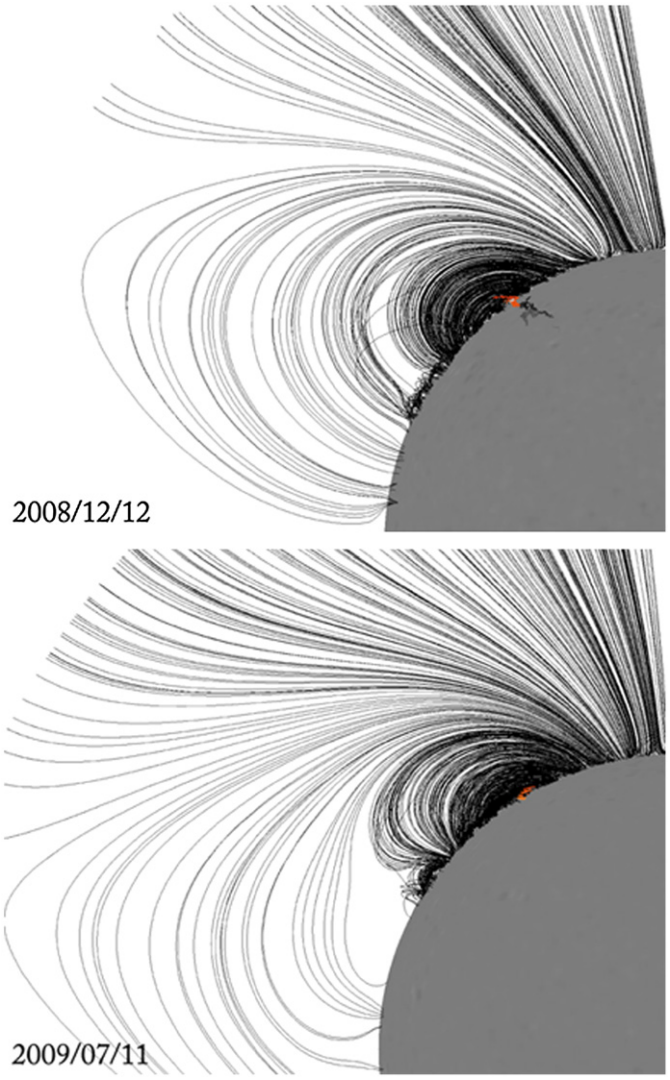

Fig. 12. PFSS extrapolation of the open solar magnetic field and the coronal loops overlying the filament before the non-radial eruptions on 2008 December 12 (top) and 2009 July 11 (bottom).

We propose the existence of two levels of deflecting forces, which have different spatial and temporal scales. During the initial phases of a prominence eruption, before the development of the CME flux-rope due to reconnection of the filament channel arcade below the filament, the filament material is seen to roll sideways compared to the radial direction. This occurs on a faster time-scale: i.e. the early rising of the filament and its rolling appear to happen before the formation of the CME, but simultaneously with the rising of the filament cavity and arcade. Later, when the overlying arcade reconnects under the filament and forms the flux rope of the future CME, we observe the bright post-eruptive arcade along the polarity reversal boundary, which forms after the reconnection. The filament sideways rolling motion begins first and is followed by the CME formation.

Since the first evidence of the roll effect can be observed during the early stages of the filament eruption, when the filament is still confined inside the cavity of the coronal arcade, we can associate this phenomenon with the local magnetic force imbalance caused by the presence of a coronal hole near the filament channel. Here we have a spatial scale difference: the roll effect depends on the imbalance of the forces inside the filament arcade that is acting on the rising filament, which is schematically illustrated in the Fig. 13 by red arrows; the CME non-radial motion is the result of the global magnetic field force imbalance. The degree and direction of the rolling motion of the filament plasma and the degree of non-radial motion of a CME, respectively, are evidence of more local and more global force imbalances occurring during the eruption. Differences in the force at different positions will result in the non-aligned propagation of erupting filament and corresponding CME.

STEREO-B/COR2 images for 2009, July 11 show the pseudostreamer (Wang et al., 2007), located above two prominences which erupted later on 2009 July 11 and 12. The direction of this pseudostreamer is 17° from radial propagation. We note that the null point in the pseudostreamer was also deflected due to imbalance between the dominant north polar coronal hole field and another smaller, weaker coronal hole. In such a case the null point will not be centered symmetrically above the two arcades. Both arcades were well developed and the base of the pseudostreamer between the two coronal holes of the same polarity in our case was twice as large as the cases described in the Wang et al. (2007). This means that the null point for the 2009, July events was located at a greater height and had less influence on the local prominence dynamics. That said, the nature of the non-radial CME propagation and local prominence dynamic such as the non-radial rolling motion is similar: the motion is towards the area with the lowest magnetic flux density. It is important to notice that the local imbalance of the forces inside the filament arcades was created, in our cases, by the presence of the coronal holes near the filament channel. It is not the only possible source for such imbalance. The presence of an active region, for example, can have the same kind of an influence on the local force distribution in the filament channel.

In general, if electro-magnetic stresses dominate the force balance during the eruption, one would expect the motion of the filament to be directed towards the least magnetic flux density region. Moreover, above and beyond the tendency of the eruption

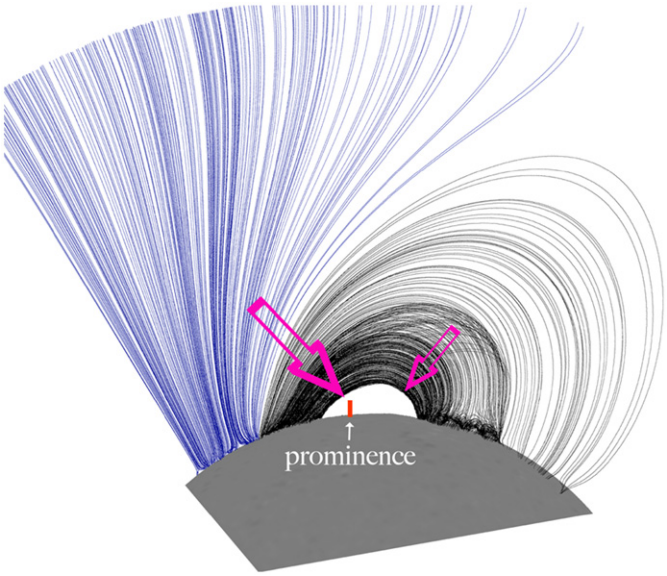

Fig. 13. The coronal hole (blue lines) near the filament channel acts as an obstacle to the expanding arcade (black lines), as the same polarity field between the filament channel and CH boundary is compressed. A diagram shows the site of the filament and location of the polarity reversal boundary (orange vertical line) relatively to the overlying magnetic arcade and open field of the coronal hole. Arrows represent the approximate relative strength and the direction of a pushing force causes the rolling of a filament ribbon during the eruption. The force is directed more sideward if the filament channel and the filament are not centered beneath the overlying arcade of coronal loops. The roll effect is expected to be more pronounced with the increase of both the force imbalance inside the arcade and the decentering of the prominence relative to the overlying coronal loop system.

to move towards the regions of less magnetic flux density surrounding the null points above the structure, there will also be a lateral deflection due to the lack of symmetry in the local magnetic fields around the polarity reversal boundary associated with the corresponding filament channel.

4.2. Relationship of roll direction with prominence chirality

In all cases of the roll effect recognized to date, there has been a one-to-one relationship between the chirality of the filament and the direction of roll with dextral filaments always rolling toward the positive photospheric magnetic field side of the prominence and sinistral filaments rolling in the opposite direction (Martin, 2003; Panasenco and Martin, 2008). These relationships hold for the events described in this paper. As we have no reason why the chirality and rolling motion should be related, this relationship might be a happenstance hemispheric association with the polarity of the adjacent coronal holes. If so, exceptions to this relationship might be found in the future.

5. Conclusions

The three erupting prominences with the roll effect had the following features in common:

(1) an association with CMEs which were non-radial in the same direction as the erupting prominence;
(2) a location above a polarity boundary adjacent and nearly parallel to a nearby coronal hole boundary ($\pm 10^{\circ}$);
(3) non-radial motion away from a nearby coronal hole; and
(4) rolling motion away from the closest coronal hole.

One erupting prominence was observed as a prominence above the limb on December 12, 2008 in EUVI 304 Å images from both STEREO-A and STEREO-B. When the prominence was modeled as a flat ribbon attached to the disk at its ends as viewed from STEREO-A, the same model also successfully reproduced the apparent shape of the prominence as viewed from STEREO-B.

Because data sets on erupting events differ greatly, three examples of quiescent prominences is too small a number to know what is typical. Many more data sets need to be studied to refine and fully understand the above relationships found between rolling motion, non-radial motions of associated CMEs, and their proximity to coronal holes. Nevertheless, this preliminary study enabled a new hypothesis for testing with larger data samples and by modeling: that the rolling motion within erupting prominences is closely related to the physical properties and the force balance of the arcade overlying the filament and nearby coronal holes in addition to the magnetic fields close to the filament, the filament channel, the filament cavity, and the developing field of the CME.

References

Cremades, H., Bothmer, V., 2004. Astronomy and Astrophysics 422, 307.
Gopalswamy, N., Shimojo, M., Lu, W., Yashiro, S., Shibasaki, K., Howard, R.A., 2003. Astrophysical Journal 586, 562.
Gopalswamy, N., Mäkelä, P., Xie, H., Akiyama, S., Yashiro, S., 2009. Journal of Geophysical Research (Space Physics) 114, A00A22.
Howard, R.A., et al., 2008. Space Science Reviews 136, 67.
Martin, S.F., 1998. Solar Physics 182, 107.
Martin, S.F., 2003. Advances in Space Research 32, 1883.
Panasenco, O., Martin, S.F., 2008. Subsurface and Atmospheric Influences on Solar Activity 383, 243.
Schrijver, C.J., De Rosa, M.L., 2003. Solar Physics 212, 165.
Wang, H., Chae, J., Gurman, J.B., Kucera, T.A., 1998. Solar Physics 183, 91.
Wang, Y.-M., Sheeley Jr., N.R., Rich, N.B., 2007. Astrophysical Journal 658, 1340.